Device

Article

Magnetically triggered ingestible capsule for localized microneedle drug delivery

Graphical abstract

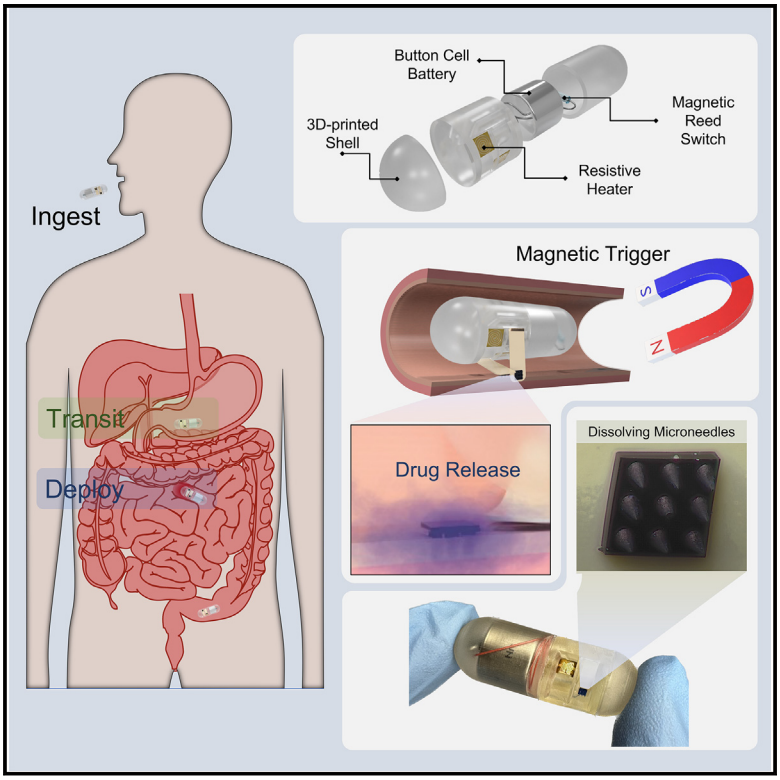

Highlights

- Capsule enables localized drug delivery via dissolving microneedle arrays
- Localized drug delivery is enabled by rapid low-power actuator deployment (<3 s)
- Thermomechanical cantilever actuator resists relaxation for high reliability
- Handheld magnet enables triggering from outside of the body

Authors

Joshua A. Levy, Michael A. Straker, Justin M. Stine, Luke A. Beardslee, Reza Ghodssi

Correspondence

ghodssi@umd.edu

In brief

Localized gastrointestinal (GI) drug delivery offers potential for enhanced treatment of GI disease. We demonstrate the use of an actuator-embedded ingestible electronic capsule to achieve localized delivery of drug-loaded microneedles. Rapid magnetic triggering is achieved via melting of a low-melt adhesive, and the rapid deployment of a cantilever actuator facilitates reliable localized delivery. This device will enable study and clinical implementation of advanced drug-delivery approaches for more effective treatment of GI disease with minimized side effects.

3 **Develop**
Prototype with demonstrated applications in relevant environment

Levy et al., 2024, Device 2, 100438
October 18, 2024
https://doi.org/10.1016/j.device.2024.100438

CellPress

Device

CellPress
OPEN ACCESS

Article

Magnetically triggered ingestible capsule for localized microneedle drug delivery

Joshua A. Levy,[1,2,3] Michael A. Straker,[2,3,4] Justin M. Stine,[2,3,5] Luke A. Beardslee,[2] and Reza Ghodssi[1,2,3,4,5,6,*]
[1]Department of Materials Science and Engineering, University of Maryland, College Park, MD 20742, USA
[2]Institute for Systems Research, University of Maryland, College Park, MD 20742, USA
[3]Robert E. Fischell Institute for Biomedical Devices, University of Maryland, College Park, MD 20742, USA
[4]Fischell Department of Bioengineering, University of Maryland, College Park, MD 20742, USA
[5]Department of Electrical and Computer Engineering, University of Maryland, College Park, MD 20742, USA
[6]Lead contact
*Correspondence: ghodssi@umd.edu
https://doi.org/10.1016/j.device.2024.100438

THE BIGGER PICTURE Gastrointestinal (GI) diseases are a widespread health challenge and are particularly hard to treat, with difficulty partially stemming from the debilitating side effects of commonly used drug treatments. A promising approach to improve patient outcomes is the use of localized drug therapy to isolate treatment of specific locations or organ systems, thereby increasing local drug concentrations and decreasing undesired side effects. In this work, we show that an ingestible actuation device triggered by an external magnet has the capacity to treat diseased sites in the intestinal tract. The developed capsule passively transits the GI tract and deploys microneedles at predetermined afflicted areas. This ingestible technology could significantly improve both efficacy and tolerability of various drug treatments, supporting new and more effective GI disease management protocols.

SUMMARY

Localized gastrointestinal (GI) drug delivery could substantially increase therapeutic efficacy for GI disorders by increasing the local concentration while reducing systemic side effects. Prior examples of localized oral drug delivery exhibited insufficient localization or reduced efficacy due to the mucosal barrier or are prohibitively complex and cumbersome for clinical practice. We demonstrate a scalable, ingestible capsule device that is remotely triggered using a handheld magnet, delivering drug-loaded microneedles to the intestinal tract in 2.91 ± 0.48 s. The system uses a resistive heating element to melt a binding adhesive, triggering deployment of cantilever actuators that insert microneedles into the intestinal tissue. Magnetic reed switches (6–10 ampere-turns [AT]) trigger the heater by closing at <1 mT field strength reliably. The demonstrated system is a major advancement for localized drug delivery and has significant potential to augment treatment of GI disorders, resulting in increased patient comfort, compliance, and treatment efficacy.

INTRODUCTION

The gastrointestinal (GI) tract of the human body interfaces with the external environment and serves the unique role of absorbing nutrients into the body through its selectively permeable mucosal barrier and densely dispersed capillary systems.[1–3] The ability of the mucosal barrier to exclude entry of many drug types based on size and chemistry is a significant challenge for oral drug delivery, despite being the preferred route by patients compared to parenteral routes (e.g., intravenous or intramuscular).[4–6] Moreover, the treatment of GI-specific disorders like inflammatory bowel disease (IBD) and intestinal cancer is still challenging as, for many orally delivered therapeutics, much of the dose is absorbed off-site and reaches the systemic circulation, causing undesirable systemic side effects.[7–10] Localized treatment targeting sites of affliction is a promising strategy to reduce overall dosing and thus drug side effects while enabling increased local concentration and efficacy.[11,12] In the GI tract, this approach can be facilitated by devices that actuate to release or inject drug into the intestinal tissue.

In recent years, ingestible devices for monitoring of the GI tract have surfaced that can perform optical, pH, temperature, and gas sensing, along with other electrochemical sensing applications.[13–23] These sensing ingestible capsules are designed to assess physiological conditions for scientific exploration and disease diagnosis. Most prominent of these examples is the PillCam, a capsular endoscope that uses a camera integrated with electronics for data communication.[24–26] Notably, ingestible

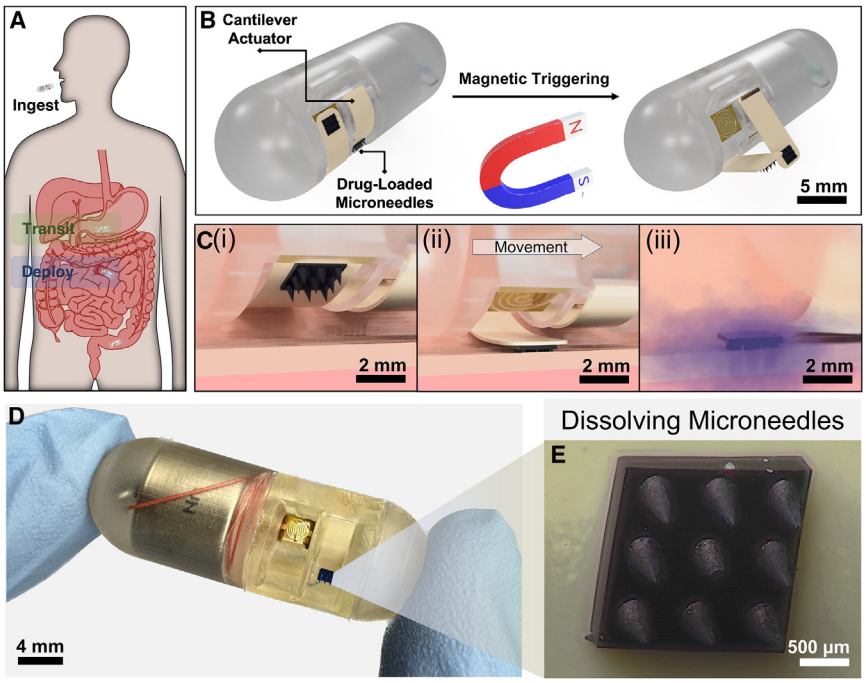

Figure 1. Depiction of the capsule operation principle

(A) Phases of capsule operation from ingestion through deployment and passing.

(B) Magnetic deployment principle showing the cantilever deploying in the presence of a magnetic field.

(C) Close-up rendering of cantilever. (i) Before deployment, (ii) during deployment of drug-loaded microneedles into tissue, and (iii) subsequent release of drug.

(D) Image of packaged capsule.

(E) Close up of the dissolving microneedle array that releases drug into the GI tissue once deployed.

devices can access the small intestine, which is largely not accessible to endoscopes.[23] These tools not only enable diagnostics, but also can locate sites and regions in need of treatment. Thus, ingestible sensing systems provide a framework for localized drug delivery; however, the tools to achieve drug localization have yet to appear in medical practice.

Advanced drug-delivery approaches for the GI tract have been developed that provide superior control over dose release characteristics. Regional-targeting pH-responsive pill coatings were developed in the 1950s; these circumvent drug release in the stomach and dissolve in the small intestine for passive targeted drug release.[4,27] Not until recently were ingestible devices developed with triggering mechanisms, like combustion and magnetic actuation, to release drug payloads on command into the intestinal lumen.[28–32] While these examples achieved localization, they failed to bypass the epithelial barrier effectively. Microneedle drug delivery in the GI tract has been shown to effectively penetrate the GI wall and release drugs into mucosal tissue to bypass the mucosal barrier.[33–35] pH-responsive and dissolvable materials have now been used as triggering mechanisms in ingestible robotic pills that passively insert micro-/milli-needles into the mucosal tissue in the stomach and small intestine.[3,33–42] These devices solve the key issue of bypassing the mucosal barrier, enabling oral delivery of biological macromolecules like insulin, yet they still suffer from a low regional targeting ability defined by pH-specific GI regions. Alternatively, combining active triggering with actuation is a straightforward technique to achieve true localization, enabling targeting of drug delivery to sites of need on command. Lee et al. recently showed a novel example of localized microneedle drug delivery using an external electromagnetic actuation (EMA) system.[43,44] However, the use of complex external electromagnetic systems is costly, requires operational expertise, and is ultimately prohibitive in a clinical or at-home setting. Our group has recently demonstrated a thermomechanical actuator for localized drug delivery in the GI tract that could achieve deployment in under 15 s.[45] Nevertheless, this example is an isolated actuator having yet to be integrated in an ingestible device and suffers from viscoelastic effects limiting the response time and deployment longevity.

In this paper, we present a magnetically controlled cantilever actuator capsule (Figure 1) that uses flexible polyether ether ketone (PEEK) cantilevers to deliver a drug payload to specific locations in the GI tract. This system is triggered by a simple circuit composed of a button cell battery in series with a magnetic reed switch and resistive heating element. When exposed to magnetic fields above ~0.5 mT, the magnetic reed switch closes, allowing current to pass through the heater, causing joule heating and melting of an adhesive ethylene vinyl acetate (EVA) layer holding the cantilever in place. Following deployment of the cantilever, the drug-loaded microneedles insert into the tissue, and the cantilever detaches from the capsule. Critically, this configuration enables deployment of the system using an innocuous nonspecific magnetic field, such as that generated by a handheld neodymium iron boron (NdFeB) magnet (Figure S1). Cantilever deployment occurs rapidly (<3 s), and PEEK exhibits excellent creep resistance to extend shelf life. Moreover, the compact and customizable nature of the actuation system makes it amenable to further multiplexing to target multiple points of interest. Overall, the demonstrated technology has the potential to bring localized drug-delivery technology to clinical practice—revolutionizing treatment efficacy and tolerability for GI disorders.

RESULTS AND DISCUSSION

Assembly and operation

Fundamentally, the cantilever actuator capsule system consists of a magnetic reed switch in series with the 2L76 button cell battery and resistive microheater to trigger actuation when exposed to a magnetic field (Figure 1B). The heater is fabricated by a standard lift-off process on a Kapton substrate (Figure S2). The reed switch is electrically joined to the battery via spot welding, and electrical connections between the heater, battery, and reed switch are

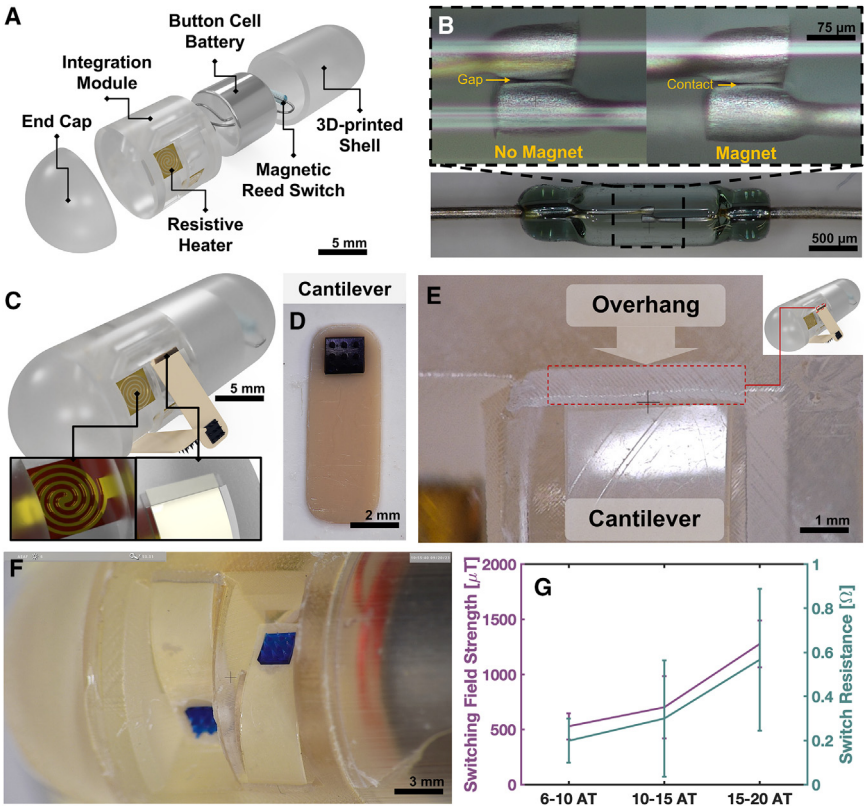

Figure 2. Design overview and magnetic triggering mechanism

(A) Computer-aided design (CAD) rendering of the system overview depicting electrical and packaging capsule components.

(B) Close up of the magnetic reed switch in the open and closed states showing the reed gap and contact, respectively.

(C) Rendered assembled capsule showing the resistive heating element and the overhang used to restrain the fixed end of the cantilever.

(D and E) The cantilever (D) and the cantilever under the overhang (E) that restrains during flexure and releases when relaxed.

(F) Magnified view of two cantilevers before deployment.

(G) Characterization of the magnetic triggering mechanism showing the switching field strength and switch resistance for different designed switching strengths (n = 3). Data are represented as the mean ± SD.

formed via soldering and silver (Ag) conductive-paste-filled channels in the cantilever module. The capsule shell directly attaches to the cantilever module and contains the battery, reed switch, and associated wiring, while the cap attaches to the other side of the module to create a rounded end shape (Figure 2A). The capsule shell, cap, and cantilever module are all 3D printed using a liquid crystal display (LCD) vat photo-polymerization (VPP) process of biocompatible resins, and the capsule is assembled by attaching the shell and caps to the cantilever module using biocompatible urethane adhesive (Figure S2). Cantilevers are attached on the fixed end using loose restraints in the module that hold during cantilever flexure but allow release after deployment. The free end of the flexed cantilever is held in place by a low-melting-point adhesive (EVA) that melts when heated by the heater. Attached to the free end of the cantilever is a 3 × 3 drug-loaded microneedle array that penetrates the intestinal tissue, releasing drug following deployment. Prior work investigating dissolving microneedles suggests that a microneedle array with needle lengths of 600 µm and spacing of 600 µm effectively penetrates and transfers drugs from microneedles into tissue.[34,46,47] The cantilever actuator is triggered by the resistive heater melting the adhesive holding the cantilever in place. Current flow through the heater is controlled by the magnetic reed switch connecting the heater and battery (Figure 2A).

Magnetic triggering

The triggering mechanism for the drug-release capsule relies on the state of the magnetic reed switch to initiate cantilever actuation. Figure 2B shows the magnetic reed switch composed of a glass package containing inert gas, ferromagnetic reeds, and leads exiting the glass package. The unperturbed open (left) and polarized closed states (right) show the gap and contact, respectively, of the two reeds. When in a magnetic field, the two ferromagnetic reeds suspended in the glass package generate temporary magnetic polarization, attracting each other and forming electrical contact. To evaluate the effectiveness of the reed switch in the given environment, this contact was assessed on the benchtop, and the required magnetic field for switching and switch resistance were evaluated. The switching field strength and switch resistance were evaluated (Figure 2G) to understand the impact of the designed switching strength, measured conventionally in ampere-turns (AT), on these characteristics. Magnetic reed switches with designed switching strength of 6–10, 10–15, and 15–20 AT exhibited ascending switching field strength as expected. The 6–10 AT switches closed at 529 ± 117 µT (n = 3), 10–15 AT switches closed at 702 ± 282 µT (n = 3), and 15–20 AT switches closed at 1,278 ± 212 µT (n = 3). This range of field strength is suitable because it exceeds commonly encountered magnetic fields but is readily achievable with handheld magnets or portable electromagnetic (EM)-generating devices. For example, the earth's magnetic field strength varies between approximately 20 and 68 µT,[48] and commercial medical equipment utilizes up to 1.5 T.[49] Moreover, these microtesla magnetic fields exhibit little magnetic force pulling on the capsule; at a 1 mT field the capsule generated <10 mN of force on the capsule, far less than that required to begin damaging intestinal tissue.[50] Notably, the switch resistance also follows a similar trend, ascending with switch strength. The immediate reason for this is unclear, although it may result from increased reed rigidity or experimental variations. While switch resistances exhibited relatively large standard deviations, the resistance remained below

1 Ω, significantly less than the heater (≥50 Ω), resulting in a negligible impact on the power dissipation of the heater. While all examined reed switches are suitable and show minimal potential for bodily harm, these results demonstrate that the 6–10 AT switch is ideal due to its lower switching field strength and switch resistance, increasing the likelihood of successful deployment.

Using the NdFeB N52 magnet shown in Figure S1, the reed switch was triggered from a distance of 11.6 ± 0.4 cm (n = 3) (Figure S9). This is sufficient to reach through the mean half-thickness of the human sagittal abdominal diameter (10.85 cm).[51] However, in cases of larger individuals, stronger magnetic fields may be required for sufficient magnetic field strength to reach the central regions of the intestinal tract. In practice, the use of a handheld electromagnet would provide sufficient field strength at greater distances to effectively trigger the actuator.

Mechanical analysis of the cantilever

The cantilever actuator stores elastic potential energy by flexure of the cantilever about the capsule circumference and is designed to deploy by melting of the adhesive EVA followed by detachment from the capsule after deployment, shown in Figure S3. Figure 2C shows a magnified view of the heater and cantilever in position, where the fixed end of the cantilever can be seen resting under the overhang in the cantilever module, enabling fixture during compression and detachment after deployment. Figure 2D shows the cantilever with attached drug-loaded microneedles, an 8.5 × 3 mm rectangular shape with 1 mm fillets to eliminate sharp edges, precluding tissue damage after deployment. The cantilever actuator relies on the internal stresses in the flexed cantilever to deploy rapidly with the appropriate force. The most important success criteria are (1) achieving rapid actuation (<5 s) to target specific locations before moving significantly due to intestinal contractions and (2) achieving suitable force to insert microneedles without damaging intestinal tissue (100–500 mN) given the 2 × 2 mm microneedle array patch.[50] To evaluate the response time and force dynamics, mechanical tests were performed by deployment of the cantilever into a load cell.

The following materials were selected for evaluation owing to their biocompatibility and known bulk mechanical properties (i.e., high modulus and resistance to stress relaxation): PEEK, cellulose acetate (AC), polyester (PES), polycarbonate (PC), and ultra-high-molecular-weight polyethylene (UHMWPE). The materials used here are well characterized in their bulk form with established mechanical properties. Nevertheless, the performance of these different materials in the context of this mechanism is not entirely predictable. Thus, evaluation in realistic conditions was conducted to understand the impact on functionality. Finite element method (FEM) models indicated that thicknesses in the range of 75–500 μm would be suitable to achieve the desired forces (Figure S4). Figures 3A–3F show the results of mechanical tests of various cantilever materials and thicknesses. For all cases, a 10 mg proof mass was used to approximate the microneedle array weight and inertial contributions without influencing the results due to dampening by the microneedle structure. Figures 3A and S5 show a representation of the deployment experiment before deployment (t < 4 s) and after deployment (t > 4 s) with the accompanying force profile for a 127 μm PEEK cantilever. Cantilever deployment occurs rapidly, resulting in a peak force higher than the equilibrium force due to the inertia of the mass and cantilever. The force then equilibrates to a steady state within milliseconds resulting from the elastic cantilever force on the load cell. While this is evident in the case of PEEK (Figure 3A), other materials tested exhibited gradual deployment and progressive force profiles on the load cell (Figure 3C). This is due to the viscoelastic properties, specifically stress relaxation, of the polymeric cantilevers. Figure 3C highlights this effect showing the difference between the rapid deployment of a PEEK cantilever and gradual deployment of a UHMWPE cantilever. For elastic applications, high viscoelastic character due to stress-induced molecular rearrangements is an inherent challenge for polymers; this is not only because it results in slow deployment, but also because the extent of relaxation changes with time, making corrections for prolonged deployment time impossible.[52] Overall, thicker cantilevers are more susceptible to stress relaxation because they are subject to higher compressive and tensile strains on the bottom and top surfaces, respectively. However, the thicker cantilevers also exhibit higher forces, as evidenced by Figures 3D and 3F comparing the deployment forces of varied thicknesses of PEEK between 76 and 508 μm (n = 3).

The challenge of stress relaxation of polymeric structures is one that has been encountered previously for miniature polymer spring deployment.[45] While polymers interface well with the soft intestinal tissue, they are susceptible to the aforementioned viscoelastic properties. To specifically assess long-term transience of deployment, cantilevers underwent prolonged bending at 130° for 72 h in a 3D-printed bending apparatus meant to emulate bending in the capsule as shown in Figure 3H. Following the 72 h, bending images revealed the residual angle of the cantilevers (Figure 3G). As expected from its high modulus and resistance to stress relaxation, PEEK outperformed other materials (PC, PES, and AC), and thicker cantilevers exhibited further relaxation. Thus, PEEK was the chosen material for this application. The 254 μm PEEK cantilevers presented the ideal balance of deployment force, 180.8 ± 17.0 mN (n = 3), and relaxation angle, only 21° over 72 h of bending. Furthermore, the 21° initial relaxation did not proceed proportionately over a 60 day period, resulting in only 32° of relaxation after the 60 days in flexure. These viscoelastic characteristics make the 254 μm PEEK cantilever an excellent choice for this application, delivering rapid deployment response and prolonged shelf life compared to prior examples of similar technologies.

Optimization of the resistive heater

The restive heating element is a critical component determining the deployment time of the cantilever actuator by melting of the EVA adhesive that holds the cantilever in flexion. Design and optimization of the heater must account for input power constraints, deployment time, and reliability. In a prior development of a similar thin-film heating mechanism,[45] the heater resistance was controlled by modifying the deposition thickness of the Au traces. To achieve the fastest deployment time with the given geometry, the resistance was tuned to ∼50 Ω based on the peak discharge current (60 mA) achievable from the 2L76 coin cell battery and assuming an ∼3 V potential difference. This

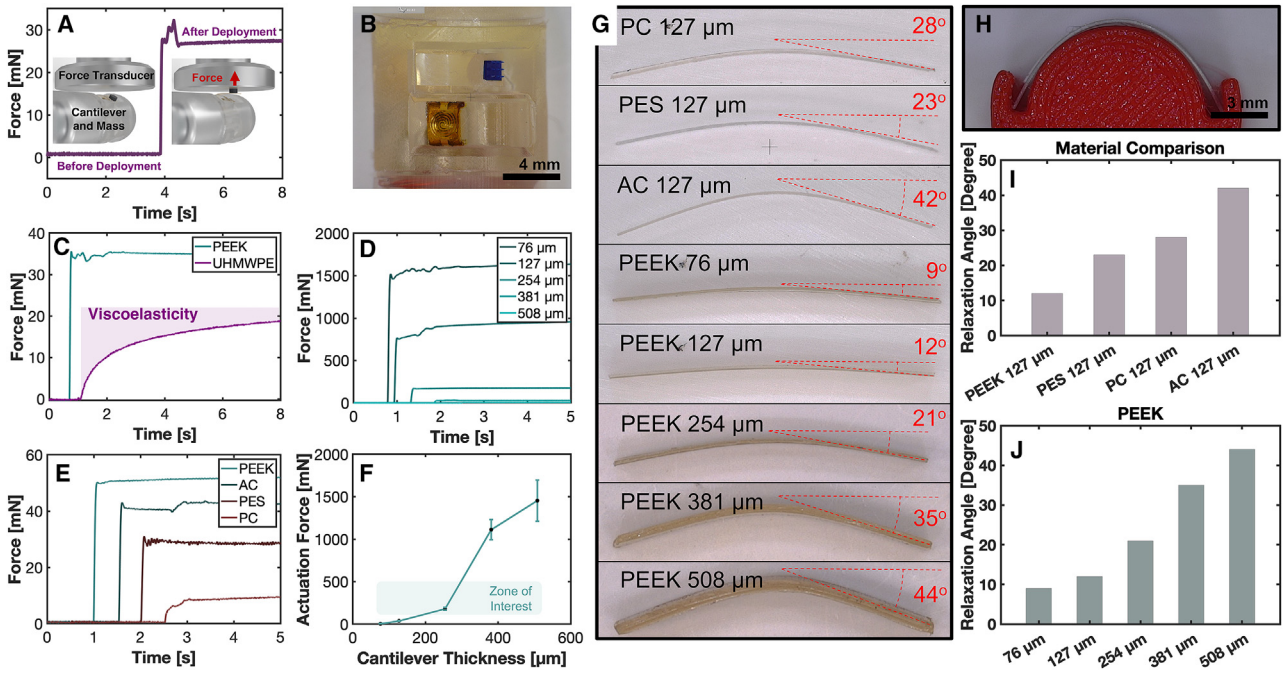

Figure 3. Mechanical analysis of the cantilever

(A) Force profile throughout deployment with representative renderings of the capsule before and after deployment into the load cell.

(B) Image of the cantilever module after deployment of one cantilever.

(C) Comparison of PEEK and UHMWPE illustrating the rapid response of the PEEK material compared to the slow viscoelastic response of the UHMWPE.

(D) Deployment profile of different PEEK thicknesses.

(E) Comparison of PEEK, AC, PES, and PC of 127 µm thickness showing the differed elastic moduli.

(F) Plot of PEEK cantilever thickness vs. actuation force between 76 and 508 µm (n = 3). Data are represented as the mean ± SD.

(G) Images of cantilevers after prolonged bending showing the residual angle. Dotted lines represent half of the residual bend angle.

(H) The bending apparatus.

(I) Comparison of relaxation angle between materials; all cantilevers have a 127 µm thickness.

(J) Comparison of relaxation angle between different thicknesses of PEEK cantilevers between 76 and 508 µm. Data are represented as the mean ± SD.

configuration resulted in the highest achievable power dissipation to achieve rapid melting of the polymer adhesive. Nevertheless, reduction of heater size and tuning of current supply could enable higher areal density of thermal dissipation, leading to faster melting, lower power consumption, and greater potential for future device miniaturization. To this end, further evaluation of case examples of heater geometry and power constraints was performed to optimize melt time, efficiency, and reliability.

Heaters were designed in six different variants, all having the same proportionate geometry, with different sizes shown in Figure 4D (outer diameter [OD] of 0.5, 1, 1.5, 2, 2.5, and 3 mm). An example of the heater with 2.5 mm OD is shown in Figure 4A before and after melting of the EVA adhesive and in Figure 4B after integration with the cantilever module of the capsule by electrical connection using conductive Ag epoxy. Due to the identical heater geometry across sizes, and thus ratio of trace length (L) to trace width (W), the resistance was expected to be the same for each variant with the same Au deposition thickness. Evaluation of the heater was performed via modeling and benchtop testing. Figure 4C shows a plot of the theoretical areal power density in mW/mm^2. At comparable resistance, smaller heaters dissipate the same amount of energy over a smaller area, leading to higher areal power density and higher heater surface equilibrium temperatures. In addition, the deposition thickness linearly impacts the cross-sectional area of the heater and thus inversely impacts the resistance. Thicker traces with lower resistance result in higher current flow and power. While higher areal power density does not linearly correlate to efficiency, smaller heaters reduce wasted thermal energy when used with smaller adhesive quantities and are expected to minimize melt time, further reducing wasted thermal energy. The areal power density also has implications on reliability, where higher temperatures seen in smaller heaters resulted in frequent electrothermal trace failures. The highest areal power density achievable with the evaluated sizes and power constraints is ~900 mW/mm^2 with a 0.5 mm heater and 150 nm trace thickness. Heaters of this configuration failed in most instances, and heaters with less than ~200 mW/mm^2 proved to be most reliable.

To identify general trends in the reliability and deployment time, the heaters were evaluated on the benchtop. Figure 4E shows the characterization of heater resistance for all sizes of a 70 nm Au trace thickness heater to illustrate trends seen across all groups. Overall, the smaller heaters were less reliable and less predictable. As can be seen in Figure 4E, the 0.5 mm heater had a mean resistance of 180.8 ± 151.9 Ω (n = 4), while the 3 mm heater had a mean resistance of 112.0 ± 1.6 Ω (n = 4). Moreover,

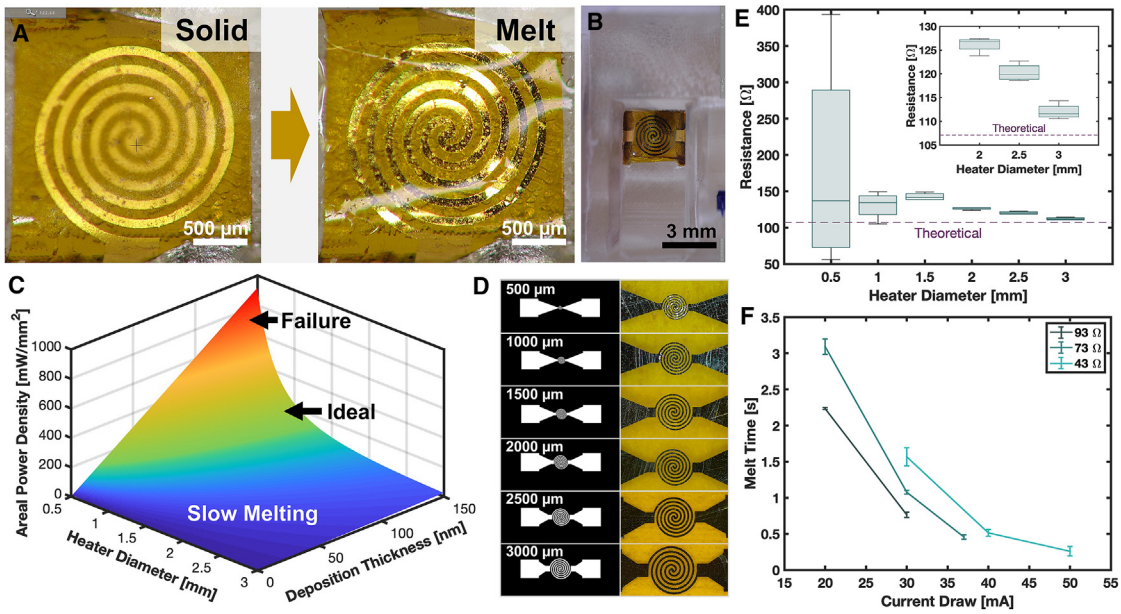

Figure 4. Optimization of the resistive heating element

(A) Transition of EVA from solid semi-crystalline translucent state to transparent melt state when heated by the heater.

(B) Heater packaged in the actuator module.

(C) A 3D map showing the areal power density of heaters as a function of heater diameter and deposition thickness.

(D) The six heater photomask designs and fabricated coils.

(E) Evaluation of heater resistance for 70 nm Au trace thickness heaters of all sizes (n = 4).

(F) Comparison of melt times for 2.5 mm heaters with deposition thicknesses of 80, 100, and 140 nm (n = 3 for all). Data are represented as the mean ± SD.

the larger heaters performed closer to the expected theoretical performance, with the 3 mm heater deviating only 4.6% from the theoretical value of 107.1 Ω predicted in Figure 4C. Thus, while the smaller heaters achieve a desirably high areal power dissipation density, the lower limit of heater size should be ~1 mm OD to minimize failure and unpredictability. To assess the impact of heater resistance on melt times, various thicknesses of 2.5 mm heaters were evaluated under controlled current using a commercial power supply regulated to 3.3 V (n = 3). As can be seen in Figure 4F, higher current draw generally resulted in faster melting; however, heaters of higher resistance performed better at a given current limitation. These results are unsurprising, but they validate that heaters of higher resistance enable balancing of energy consumption and deployment time. These results indicate that the ideal heater configuration to achieve deployment in less than 1 s with minimized power consumption is a size between 1 and 2.5 mm and a trace thickness of ≤80 nm. Deployment in 3 s supports precise sub-millimeter delivery location targeting in the intestinal tract considering a mean intestinal translation speed of 1.4 cm/min.[53]

Benchtop and *ex vivo* validation of drug delivery

To assess the performance of the localized drug-delivery capsule in a realistic environment, the actuator was deployed while submerged in 1× phosphate-buffered saline (PBS) solution and in a porcine *ex vivo* intestinal environment. Figure 5A shows the capsule undergoing testing while submerged to verify its resilience to operation in an aqueous environment like the gut. The capsule was placed in a beaker and submerged, then a handheld NdFeB magnet was used to trigger the actuation of the cantilever. No solution was observed to permeate the capsule shell over the course of 1 h, and the cantilever actuator deployed in <3 s after introduction of the magnet within 10 cm of the capsule. Full submersion is intended to simulate an extreme case of full submersion in the intestine, as the capsule will likely encounter a combination of liquid and gaseous media in transit through the esophagus, stomach, and small intestine. While this demonstration confirmed that actuator deployment is possible while fully submerged, protection of the drug-loaded microneedle array was not demonstrated. Previously, our research group has demonstrated a freestanding bilayer for protection of active components of an ingestible device.[54] In the future, we will use this bilayer to protect the microneedles from premature drug release.

Deployment of the capsule in *ex vivo* intestinal tissue is intended to simulate close-to-realistic conditions expected at the interface between the cantilever, the microneedles, and the gut environment. In general, the small intestine contracts to surround contained materials and promote motility; thus, the capsule is expected to be oriented axially and in proximity of the intestinal wall at most points in time. Moreover, as designed, the cantilevers can protrude 4 mm from the capsule surface, adding to the 13 mm diameter of the capsule. This extension to 17 mm from the opposite side of the capsule nearly fills the ~25 mm diameter of the small intestine.[53] In some cases, the capsule could be oriented toward the lumen, prohibiting

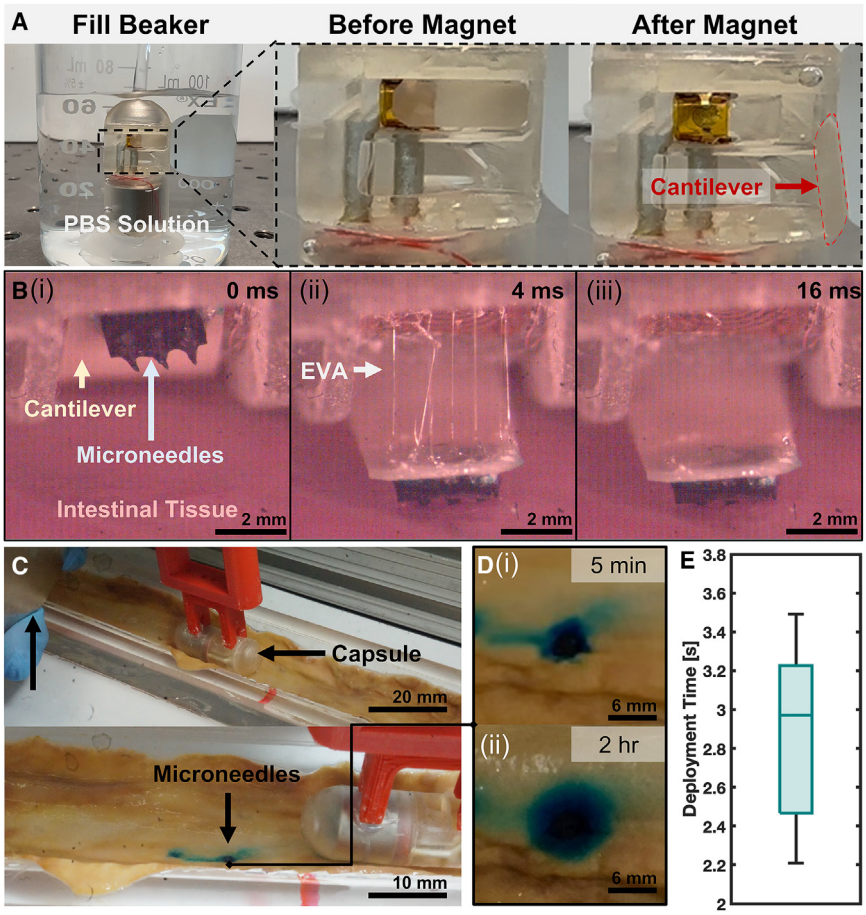

Figure 5. Deployment of the integrated system in an *ex vivo* GI simulator

(A) Deployment of the cantilever actuator while submerged in solution. The capsule is placed in a beaker and then filled with solution and deploys after the magnet nears the capsule.

(B) (i–iii) Deployment of the drug-delivery cantilever in *ex vivo* intestinal tissue filmed by a high-speed camera through the 16 ms of deployment activity.

(C) Evaluation of deployment in a simulated *ex vivo* environment with controlled translation speed and interfacial forces. A magnetic field was introduced with a handheld magnet and then deployment was observed.

(D) (i) The microneedle array 5 min after deployment into the intestinal tissue, showing an ~5 mm diffusion diameter. (ii) The microneedle array 2 h after deployment with an ~10 mm dye diffusion diameter.

(E) Box-and-whisker plot describing cantilever deployment time (n = 7). Data are represented as the mean ± SD.

the microneedles from contacting intestinal tissue with sufficient force, as the cantilever applies less force at greater extension. The authors will assess the occurrence of this possibility in future *in vivo* evaluations and modify the cantilever geometry to provide sufficient reach and force independent of capsule orientation. The microneedle penetration into intestinal tissue was characterized using a high-speed camera to better understand the interaction of the actuated cantilever and microneedles with intestinal tissue during deployment (Figure 5B). Further visualization of needle insertion into an agarose tissue phantom can be seen in Figures S6 and S7. Figures 5Bi–5Biii show frames from the 1,000 fps video of deployment of the actuator and microneedles into *ex vivo* porcine small intestinal tissue after the EVA adhesive begins to melt. In Figure 5Bi (t = 0 ms), the cantilever with attached microneedles is in the flexed state attached to the heater. After 4 ms (Figure 5Bii), the cantilever has almost fully deployed, showing stringing of the EVA adhesive that previously held the cantilever in flexure. After a total of 16 ms, the cantilever is fully deployed, and the drug-loaded microneedles (Figure 5Biii) have penetrated the surface of the tissue. Thus, considering individual characterization, the total deployment time was estimated as a combination of the 500–1,000 ms heater melt time and the 16 ms cantilever motion. However, in experimentation with magnetic control, the capsule exhibited deployment in 2.91 ± 0.48 s (n = 7) (Figure 5E). This deviation from the expected deployment time is believed to be due to a combination of switch and system inefficiencies, such as internal resistance and thermal dissipation to the surrounding aqueous medium. Nevertheless, an 85% reduction in deployment time was exhibited compared to the prior actuation prototype demonstrated in literature,[45] enabling significantly greater location targeting and longevity.

Following the close-up analysis of deployment in a static *ex vivo* environment, the localized drug-delivery capsule was evaluated on a custom GI simulator described in Straker et al.[54] The simulator is composed of a compliant polydimethylsiloxane (PDMS) tissue bed molded to a curvature of r = 12.5 mm and a screw-rod translation system for capsule mounting. Tissue is adhered to the surface of the PDMS bed during testing, thus adopting the approximate curvature of the small intestine. The speed of transit was controlled to 1.4 cm/min, the mean translation speed in the small intestine.[53] The capsule mount has vertical freedom, allowing mass loading to control the force on the capsule and approximate peristaltic and segmentation contractions of the gut. During translation, a magnet was used to trigger deployment of the cantilever, leaving the dye-loaded microneedle array behind (Figure 5C). Following detachment of the microneedles via rapidly dissolving PEG polymer, the release of dye was monitored over the course of 2 h. Figure 5D shows the microneedle array 5 min after deployment, and after 2 h the dye spread was observed at a diameter of ~10 mm from the 2 × 2 mm needle array (Figure 5Dii). While drug release occurs over the course of approximately 8 days from the polyvinyl alcohol (PVA) needle array, material variation allows tailoring of the drug release rate and array longevity in the future. The model drug was observed to marginally spread from the delivery location through liquid channels on the surface of the tissue. Given

the orientation of the experiment, gravity did not play a large role in transport, but future *in vivo* studies will assess the impact of orientation on delivery efficacy. Overall, this level of confinement enables significantly higher drug concentrations with minimized dosing. For example, with 1% of the drug loading of a small-intestine-targeted oral tablet, this delivery system can achieve ~380× areal drug concentration at sites of need compared to broad distribution across the surface area of the intestinal tract.[55] The mass of the microneedle arrays is 0.88 ± 0.22 mg (n = 4) as determined by analytical balance. Most drugs for treatment of IBD, like the corticosteroid budesonide (1.28 g/cm^3), have a similar or higher density compared to the PVA needles (1.19 g/cm^3); thus, a needle array loaded with a 50% w/w drug and binder mixture is expected to provide approximately 500 μg of drug in a single dose.[56,57] For comparison, a common dose of the oral corticosteroid budesonide for IBD treatment is 9 mg, which spreads throughout a large portion of the intestinal tract. Thus, given the localization of delivery, the microneedle array far exceeds the drug concentrations achievable from standard drug tablets.

At present, the most localized form of oral dosing in medical practice is enteric-coated pills that dissolve in pH > 6 following passage through the stomach. These coatings dissolve in a time frame of 15–45 min following the swift pH change in the small intestine; however, they provide no control over delivery location beyond this.[58] A lesion would need to be conveniently located in the duodenum or early jejunum to be effectively treated. Even still, the level of localization of locally delivered microneedle arrays far exceeds that of a transiting pill. While uncontrollable factors like diffusion and turbulence in the gut will attenuate the level of localization demonstrated here, this illustrates the potency of such an approach to improve local treatment while significantly mitigating systemic drug exposure and side effects.

The technology demonstrated here has the potential to significantly improve care for patients suffering from GI and systemic disease. This fully operational capsule system for targeted drug delivery into intestinal tissue using harmless microneedles is the first example of its kind that does not require complex external EMA systems—facilitating better reliability and implementation in clinical practice. The device demonstrated here is currently 13 mm in diameter, and all components have the potential for miniaturization using smaller cantilevers and smaller batteries of a higher voltage arrangement enabling even faster deployment. All critical components, including the cantilever, microneedles, heater, and packaging, are readily scalable, meaning multiplexing of actuators could allow numerous treatment events in one pass using simple electronic switching schemes. We envision that the current device could be used in cooperation with exogenous screening devices like the PillCam to locate disease sites for treatment and ultrasound or fluoroscopy tools to locate the drug-delivery capsule. These exogenous tools will inform the placement of the magnetic field source, and triggering will be achieved with magnetic fields created by handheld magnets, electromagnets, and other tools like directed magnetic fields. However, the future of ingestible devices is inevitably characterized by autonomous identification and on-site action, where onboard sensing, imaging, and electronics technology enables closed-loop control of systems like this drug-delivery cantilever actuator. Thus, operation from a single 3 V battery here is not only simple, but also allows for potential integration with other electronic capsular systems, such as sensors and communication modules that are often regulated to 3.3 V. All materials used externally on the device are ISO 10993-5 biocompatible, including the packaging, Kapton, Au, EVA, PEEK, and PVA. Moreover, the forces generated by the magnetic field on the capsule are innocuous (<10 mN), and the cantilever deployment force is tailored to minimize tissue damage.

Overall, the technology here has potential to operate as a standalone device and could also be easily modified to be used for multilocation treatment in combination with other microsystem technologies to facilitate more effective treatment of localized and systemic disease. Future development of the device will involve *in vivo* testing and scaling of fabrication processes. The fabrication approaches used here combine low-cost commercially available supplies with scalable custom manufacturing technologies. The PEEK cantilever material, battery, reed switch, and wiring are commercially available at large scale. The heater and microneedles are also fabricated with proven scalable microfabrication and micromolding processes, respectively. While capsule shells are fabricated by 3D printing, the use of injection molding would provide an alternative approach that is compatible with mass manufacturing at low cost. Investigation of compact and user-friendly magnetic triggering tools will also be key to the success of this technology. While triggering of the actuator was demonstrated using a disk magnet in this work, the use of a handheld electromagnet may enable superior control and verification of delivery.

An in-depth analysis of the triggering effectiveness of various magnet types will be performed *in vivo* in the future to optimize magnetic control. Remaining biosafety challenges prior to clinical application include assessing package biocompatibility and long-term fluid resistance. Future testing will include *in vitro* biocompatibility testing and prolonged submersion in simulated intestinal fluids to ensure that the capsule is safe for *in vivo* studies. Future *in vivo* evaluation will seek to understand the efficacy of localized drug delivery in comparison with standard coated drug tablets. Porcine models will be used in fed and fasted states to assess the significance of food and liquid on delivery performance. The performance of microneedles with different interspacing and length will be evaluated *in vivo* in different GI locations to understand their impact on delivery efficiency. While not experienced in *ex vivo* experimentation, the entrance of tissue, solids, or liquids into the actuator cavity is a potential challenge *in vivo*. Modification of the actuator recess distance and employment of the freestanding region-responsive bilayer presented in prior work is expected to preclude this possible failure point.[54] This freestanding structure is capable of both chemical and mechanical protection of the underlying components. However, after passive dissolution of the freestanding structure, there is a possibility of premature dissolution of the drug-loaded microneedles and unintended contact with the intestinal tissue. Further evaluation of this concern will be conducted in future *in vivo* testing of the device. Determining the optimal site of drug administration is another key challenge

that will be evaluated during future *in vivo* development of the device. One possible method for locating diseased sites is the use of video capsule endoscopy. This is a demonstrated approach to identify disease in the GI tract. Moreover, future ingestible sensing devices could be used with the localized drug-delivery capsule to locate sites of disease.[18,21,22] Another possibility is the use of confined magnetic fields to promote triggering in a known location. This method could be achieved by confining the field of the required triggering strength to a region of known disease. The *in vivo* investigations of efficacy will serve to confirm the evidence of enhanced efficacy of localized drug delivery, providing a path forward for clinical adoption of this technology. This work establishes a first of its kind example of a capsular technology for highly localized drug delivery in the GI tract, wherein realization of more compact packaging with scalable fabrication approaches will pave the way for repeated *in vivo* evaluation of localized GI drug delivery toward implementation in human medicine.

Conclusion

In this work, we demonstrate the first example of a remotely triggerable local drug injection system for the GI tract, establishing the potential for localized drug delivery for treatment of intestinal disease and targeted systemic dosing to advantageous sites. The magnetically triggered ingestible capsule device showed the capacity to be triggered in 2.91 ± 0.48 s and apply a force of 180.8 ± 17.0 mN with a 254-μm-thick PEEK cantilever to minimize tissue damage while sufficiently inserting microneedle drug patches. The PEEK material demonstrated excellent deployment longevity, relaxing only 21° after 72 h of bending and 11° further after 60 days beyond this point, indicating excellent shelf life and robustness for this technology. The 6–10 AT reed switch showed the ability to switch at sub-millitesla field strength, which can be readily achieved by handheld magnetic devices and is approximately 1/1,000 that used in clinical imaging applications. The optimized heater characteristics enable more rapid and efficient deployment for multiplexed actuation using simple electronic switching in the future and potentiate miniaturization and integration with other power-consuming sub-systems like sensors. These advances over prior systems enable direct control via magnets, better localization due to the fast response time, adaptability, and enhanced efficiency through localized microneedle drug release. Overall, this low-cost scalable technology brings a new opportunity for targeted treatment to specific organ systems and pathological sites in the GI tract, enabling more effective treatment with lessened adverse side effects for patients.

EXPERIMENTAL PROCEDURES

Resource availability

Lead contact

Requests for further information and resources should be directed to and will be fulfilled by the lead contact, Reza Ghodssi (ghodssi@umd.edu).

Materials availability

This study did not generate any new unique reagents.

Data and code availability

All data and code generated from this study are available upon reasonable request to the lead contact, Reza Ghodssi (ghodssi@umd.edu).

Resistive heater fabrication and evaluation

Resistive heating elements are used to melt the EVA polymer adhesive holding the cantilever in place. The heater demonstrated here has the same geometry as that presented in Levy et al.,[45] with varied scale and deposition thickness to achieve different thermal dissipation density and resistance, respectively. Heaters were fabricated by lithography using Shipley S1813 and electron beam evaporation deposition of 20 nm Cr (Angstrom, Kitchener, ON, Canada) followed by Au of varied thickness between 30 and 150 nm. Lift-off of the resist was performed by 30 min of sonication in acetone. The OD of the coil was varied between 500 μm and 3 mm to optimize heating of the EVA adhesive and reliability. MathWorks MATLAB (Natick, MA, USA) was used to evaluate the dissipation power for heaters of different sizes and thicknesses regulated to 3 V. Trace resistance was determined using trace geometry, the resistivity of Au (ρ_{Au} = 2.44 × 10^{-8} Ω m), and a previously determined correction factor for a Au heating element.[45,59] Power dissipation was calculated via Ohm's law as described in Table S1. Resistance of fabricated heaters was measured (n = 4) and compared to understand differences in fabrication repeatability between sizes. Melt time of the 2.5 mm heater (n = 3) was assessed with varied resistances and current constraints as represented in Figure 4F.

Package fabrication and assembly

The capsule system is composed of an Energizer 2L76 battery (St. Louis, MO, USA) in series with a magnetic reed switch and the thin-film resistive heating element, packaged in a 3D-printed housing with attached drug-delivery cantilevers. The module housing the heater and cantilevers was fabricated using a Phrozen Sonic Mini 8K (Hsinchu City, Taiwan) LCD VPP 3D printer with FormLabs Surgical Guide v.2 Resin (Somerville, MA, USA). The module has a 13 mm OD and contains four opposingly oriented recesses to hold the cantilevers below the surface of the capsule before deployment. The recesses have a maximum depth of 3 mm and a width of 3.5 mm, with an overhang on the fixed end of the cantilever to affix the cantilever when tensioned. The module also has ∅ = 1.5 mm channels leading from heater to the battery cavity, which are filled with MG Chemicals 8330S conductive epoxy (Burlington, ON, Canada) to form the electrical interconnects between the heater and the battery. Before curing of the Ag-filled epoxy, heaters were placed in the module and 36 AWG insulated wires were inserted into the battery end of the channels. The Littlefuse 6–10 AT normally open reed switch (Chicago, IL, USA) and battery were fused by spot welding using a Ni tab and then soldered to the heater wires. The capsule shell and end cap were fabricated via LCD VPP with a 700 μm wall thickness. The battery and wires were placed in the shell, and the shell and end cap were affixed to the cantilever module with Henkel Loctite UK M-11FL medical device urethane adhesive (ISO 10993-5 Biocompatibility; Düsseldorf, Germany).

Microneedle molding

Microneedles were molded in an 11 × 11 microneedle mold produced by Blueacre Technology (Dundalk, County Louth, Ireland) as described previously by Levy et al.[45] The mold contains 121 microneedles spaced by 600 μm on center, with a 300 μm base diameter and a 600 μm height. A 20% w/v solution of PVA (M_w 31–50 kDa) from Sigma Aldrich (St. Louis, MO, USA) containing FD&C blue no. 1 dye was poured over the mold and then exposed to near vacuum (~0.03 atm) to evacuate air from the needle mold. The array was then brought to atmospheric pressure and allowed to dry for 24 h to remove the water and cast the PVA into the mold. The molded 11 × 11 array is shown in Figure S8. Microneedle arrays were removed from the mold and segmented into separate 3 × 3 arrays for demonstration.

Cantilever actuator assembly

Cantilevers were made from commercially available polymeric films purchased from McMaster-Carr Supply (Elmhurst, IL, USA). PEEK, AC, PES, PC, and UHMWPE were chosen for their biocompatibility and evaluated for mechanical characteristics. The cantilevers were 3 × 8.5 mm and had 1 mm filleted corners to reduce the chance of bowel damage after deployment. The shape of the cantilever was laser engraved on the film surface using the Glowforge Pro laser cutter (Seattle, WA, USA) and then cut to size. As depicted in Figure S2, the cantilevers were then tucked into the slot on the fixed end of the recess in the cantilever module. Five hundred micrograms of EVA adhesive

(The Gorilla Glue Company, Sharonville, OH, USA) was melted on the heater by flowing current, then the cantilever was flexed and attached to the heater while the EVA was in a melt state. Following solidification, the cantilever remained affixed to the heater until deployment via remelting. After the cantilever was affixed, a 3 × 3 microneedle array was attached to the cantilever using ~1.5 μg of the water-soluble polymer polyethylene glycol (PEG; Sigma Aldrich, St. Louis, MO, USA) in melt form.

Reed switch evaluation

Reed switches of different switching field strength were purchased from DigiKey (Thief River Falls, MN, USA) and tested to determine the dependence of required field strength for switching and closed resistance on the designed switching strength. Littlefuse (Chicago, IL, USA) switches designed to close at 6–10, 10–15, and 15–20 AT were evaluated using a permanent NdFeB magnet at variable distance and magnetometer readout. The magnets used in the experimental procedures were N52 grade NdFeB through-diameter magnetized permanent magnets. In experimentation, two stacked magnets were used, each having a 3″ diameter and 1/8″ thickness, making a total thickness of 1/4″. Each magnet had a flux density of 14,800 G, and the total weight was 220 g as determined by the product data sheet. Reed switches (n = 3) were placed adjacent to the magnetometer and connected to a multimeter. The magnet was moved closer to the switch until electrical continuity was registered, and the field strength value was recorded. Once open, the switch resistance was measured (n = 3) to evaluate the impact of switch resistance on current flow in the packaged capsule.

Mechanical and relaxation characterization

To determine the deployment force, dynamics, and proneness to stress relaxation predicting long-term reliability, the cantilevers were evaluated using an Instron 5942 ultimate testing machine (UTM; Norwood, MA, USA) with a 5 N load cell and a custom 3D-printed mandrel with a 5 mm radius of curvature. Based on bulk mechanical properties, the following materials and thicknesses were evaluated (n = 3 for all): PEEK (76, 127, 254, 381, and 508 μm), UHMWPE (254 and 508 μm), HDPE (406 and 584 μm), PP (406 and 508 μm), AC (127 μm), PES (127 μm), and PC (127 μm). Cantilevers were deployed into the UTM load cell held 1 mm from the surface of the capsule. The force was measured and plotted for a variety of material combinations to reveal the profile and magnitude of the deployment force.

Using a custom bending apparatus, the long-term reliability of the most promising cantilever materials and thicknesses was evaluated. The test cantilevers were held at 130° bend angle for 72 h and then removed from the mandrel fixture and imaged to assess the residual bending of each material and thickness variant to indicate the level of stress relaxation and its hindrance to long-term reliability.

Ex vivo microneedle deployment

The capsule was first deployed while submerged in 1× PBS solution to evaluate water tightness and the ability to deploy while submerged. The actuator was then deployed on a static porcine *ex vivo* small intestinal tissue to evaluate deployment timing and microneedle penetration in tissue. Porcine tissue was acquired, from Animal Biotech Industries (Doylestown, PA, USA), frozen from postmortem animals. The deployment and insertion of microneedles into tissue were evaluated using a Chronos 2.1HD high-speed camera (Kron Technologies, Burnaby, BC, Canada). Following static deployment, the capsule was deployed on an *ex vivo* tissue simulator to validate the performance in a simulated environment. The tissue experiment utilized a GI simulator previously developed by Straker et al.[54] to support the intestinal tissue, provide relevant forces, and provide movement to simulate peristaltic and segmentation contractions in the intestinal tract. Translation of 1.4 cm/min was used to simulate the average transit speed in the small intestine, and a force of 500 mN exerted by 51 g of mass approximated the force expected in the small intestine.[53] During translation of the assembled capsule, the permanent NdFeB magnet was moved close to the actuator capsule and deployment was monitored following a 10 s hold in proximity of the capsule. Microneedle drug release in the tissue was tracked over a 2 h period.

SUPPLEMENTAL INFORMATION

Supplemental information can be found online at https://doi.org/10.1016/j.device.2024.100438.

ACKNOWLEDGMENTS

This work was supported by the National Science Foundation ECCS Program under award #1939236. The authors also acknowledge support from the Clark Doctoral Fellows Program, TerrapinWorks, and the University of Maryland NanoCenter and its FabLab.

AUTHOR CONTRIBUTIONS

J.A.L., L.A.B., and R.G. were responsible for conceiving the research. J.A.L., M.A.S., and J.M.S. carried out the device fabrication, experimentation, and data analysis. J.A.L. wrote the original draft of the manuscript. M.A.S., J.M.S., L.A.B., and R.G. participated in review and editing of the manuscript. R.G. supervised the research. All authors actively participated in interpretation of experimental results.

DECLARATION OF INTERESTS

The authors have filed a provisional patent application based on the idea presented in this paper.

Received: March 6, 2024
Revised: May 28, 2024
Accepted: June 6, 2024
Published: July 2, 2024

REFERENCES

1. Volk, N., and Lacy, B. (2017). Anatomy and Physiology of the Small Bowel. Gastrointest. Endosc. Clin. N. Am. *27*, 1–13. https://doi.org/10.1016/j.giec.2016.08.001.
2. Geboes, K., Geboes, K.P., and Maleux, G. (2001). Vascular anatomy of the gastrointestinal tract. Best Pract. Res. Clin. Gastroenterol. *15*, 1–14. https://doi.org/10.1053/bega.2000.0152.
3. Chu, J.N., and Traverso, G. (2021). Foundations of gastrointestinal-based drug delivery and future developments. Nat. Rev. Gastroenterol. Hepatol. *19*, 219–238. https://doi.org/10.1038/s41575-021-00539-w.
4. Alqahtani, M.S., Kazi, M., Alsenaidy, M.A., and Ahmad, M.Z. (2021). Advances in Oral Drug Delivery. Front. Pharmacol. *62*, 618411. https://doi.org/10.3389/FPHAR.2021.618411.
5. Xia, D., Wood-Yang, A.J., and Prausnitz, M.R. (2022). Clearing away barriers to oral drug delivery. Sci. Robot. *7*, eade3311. https://doi.org/10.1126/SCIROBOTICS.ADE3311.
6. Ensign, L.M., Cone, R., and Hanes, J. (2012). Oral Drug Delivery with Polymeric Nanoparticles: The Gastrointestinal Mucus Barriers. Adv. Drug Deliv. Rev. *64*, 557–570. https://doi.org/10.1016/J.ADDR.2011.12.009.
7. Thomas, R.M., and Sobin, L.H. (1995). Gastrointestinal Cancer. Cancer *75*, 154–170. https://doi.org/10.1002/1097-0142.
8. Bernstein, C.N. (2015). Treatment of IBD: Where we are and where we are going. Am. J. Gastroenterol. *110*, 114–126. https://doi.org/10.1038/AJG.2014.357.
9. Crohn's & Colitis Foundation Understanding IBD Medications and Side Effects. https://www.crohnscolitisfoundation.org/sites/default/files/2019-10/understanding-ibd-medications-brochure-final-online2.pdf.
10. Stallmach, A., Hagel, S., and Bruns, T. (2010). Adverse effects of biologics used for treating IBD. Best Pract. Res. Clin. Gastroenterol. *24*, 167–182. https://doi.org/10.1016/J.BPG.2010.01.002.
11. Eder, P., Zielińska, A., Karczewski, J., Dobrowolska, A., Słomski, R., and Souto, E.B. (2021). How could nanobiotechnology improve treatment outcomes of anti-TNF-α therapy in inflammatory bowel disease? Current

knowledge, future directions. BioMed Central *19*, 346. https://doi.org/10.1186/s12951-021-01090-1.

12. Gareb, B., Otten, A.T., Frijlink, H.W., Dijkstra, G., and Kosterink, J.G.W. (2020). Review: Local tumor necrosis factor-α inhibition in inflammatory bowel disease. Pharmaceutics *12*, 539. https://doi.org/10.3390/pharmaceutics12060539.
13. Becker, D., Zhang, J., Heimbach, T., Penland, R.C., Wanke, C., Shimizu, J., and Kulmatycki, K. (2014). Novel Orally Swallowable IntelliCap®Device to Quantify Regional Drug Absorption in Human GI Tract Using Diltiazem as Model Drug. Ageing Int. *15*, 1490–1497. https://doi.org/10.1208/S12249-014-0172-1/FIGURES/10.
14. YAMASUE, K., HAGIWARA, H., TOCHIKUBO, O., SUGIMOTO, C., and KOHNO, R. (2012). Measurement of Core Body Temperature by an Ingestible Capsule Sensor and Evaluation of its Wireless Communication Performance. Advanced Biomedical Engineering *1*, 9–15. https://doi.org/10.14326/ABE.1.9.
15. Thwaites, P.A., Yao, C.K., Maggo, J., John, J., Chrimes, A.F., Burgell, R.E., Muir, J.G., Parker, F.C., So, D., Kalantar-Zadeh, K., et al. (2022). Comparison of gastrointestinal landmarks using the gas-sensing capsule and wireless motility capsule. Aliment. Pharmacol. Ther. *56*, 1337–1348. https://doi.org/10.1111/APT.17216.
16. Kalantar-Zadeh, K., Berean, K.J., Ha, N., Chrimes, A.F., Xu, K., Grando, D., Ou, J.Z., Pillai, N., Campbell, J.L., Brkljača, R., et al. (2018). A human pilot trial of ingestible electronic capsules capable of sensing different gases in the gut. Nat. Electron. *1*, 79–87. https://doi.org/10.1038/s41928-017-0004-x.
17. Stine, J.M., Botasini, S., Beardslee, L.A., Levy, J.A., and Ghodssi, R. (2022). Miniaturized Capsule System for Hydrogen Sulfide Detection in the Gastrointestinal Tract. In Hilton Head Workshop 2022: A Solid-State, Sensors, Actuators, and Microsystems Workshop.
18. Stine, J.M., Ruland, K.L., Beardslee, L.A., Levy, J.A., Abianeh, H., Botasini, S., Pasricha, P.J., Ghodssi, R., Stine, J.M., Ruland, K.L., et al. (2024). Miniaturized Capsule System Toward Real-Time Electrochemical Detection of H2S in the Gastrointestinal Tract. Adv. Healthcare Mater. *13*, 2302897. https://doi.org/10.1002/ADHM.202302897.
19. Goffredo, R., Accoto, D., Santonico, M., Pennazza, G., and Guglielmelli, E. (2015). A smart pill for drug delivery with sensing capabilities. In Proceedings of the Annual International Conference of the IEEE Engineering in Medicine and Biology Society, EMBS 2015-November, pp. 1361–1364. https://doi.org/10.1109/EMBC.2015.7318621.
20. Liu, S., Chu, S., Beardslee, L.A., and Ghodssi, R. (2020). Hybrid and Passive Tissue-Anchoring Mechanism for Ingestible Resident Devices. J. Microelectromech. Syst. *29*, 706–712. https://doi.org/10.1109/JMEMS.2020.2999448.
21. Banis, G.E., Beardslee, L.A., Stine, J.M., Sathyam, R.M., and Ghodssi, R. (2019). Gastrointestinal Targeted Sampling and Sensing via Embedded Packaging of Integrated Capsule System. J. Microelectromech. Syst. *28*, 219–225. https://doi.org/10.1109/JMEMS.2019.2897246.
22. Beardslee, L.A., Banis, G.E., Chu, S., Liu, S., Chapin, A.A., Stine, J.M., Pasricha, P.J., and Ghodssi, R. (2020). Ingestible Sensors and Sensing Systems for Minimally Invasive Diagnosis and Monitoring: The Next Frontier in Minimally Invasive Screening. ACS Sens. *5*, 891–910. https://doi.org/10.1021/ACSSENSORS.9B02263/ASSET/IMAGES/LARGE/SE9B02263_0003.JPEG.
23. Hosoe, N., Takabayashi, K., Ogata, H., and Kanai, T. (2019). Capsule endoscopy for small-intestinal disorders: Current status. Dig. Endosc. *31*, 498–507. https://doi.org/10.1111/DEN.13346.
24. American Society for Gastrointestinal Endoscopy Standards of Practice Committee; Shergill, A.K., Lightdale, J.R., Bruining, D.H., Acosta, R.D., Chandrasekhara, V., Chathadi, K.V., Decker, G.A., Early, D.S., Evans, J.A., et al. (2015). The role of endoscopy in inflammatory bowel disease. Gastrointest. Endosc. *81*, 1101–1121.e213. https://doi.org/10.1016/J.GIE.2014.10.030.
25. Moore, L.E. (2003). The advantages and disadvantages of endoscopy. Clin. Tech. Small Anim. Pract. *18*, 250–253. https://doi.org/10.1016/S1096-2867(03)00071-9.
26. Spiceland, C.M., and Lodhia, N. (2018). Endoscopy in inflammatory bowel disease: Role in diagnosis, management, and treatment. World J. Gastroenterol. *24*, 4014–4020. https://doi.org/10.3748/WJG.V24.I35.4014.
27. Hua, S. (2020). Advances in Oral Drug Delivery for Regional Targeting in the Gastrointestinal Tract - Influence of Physiological, Pathophysiological and Pharmaceutical Factors. Front. Pharmacol. *11*, 524. https://doi.org/10.3389/FPHAR.2020.00524/BIBTEX.
28. Yim, S., Goyal, K., and Sitti, M. (2013). Magnetically Actuated Soft Capsule With the Multimodal Drug Release Function. IEEE ASME Trans. Mechatron. *18*, 1413–1418. https://doi.org/10.1109/TMECH.2012.2235077.
29. Dietzel, C.T., Richert, H., Abert, S., Merkel, U., Hippius, M., and Stallmach, A. (2012). Magnetic Active Agent Release System (MAARS): Evaluation of a new way for a reproducible, externally controlled drug release into the small intestine. J. Contr. Release *161*, 722–727. https://doi.org/10.1016/J.JCONREL.2012.04.047.
30. Yu, W., Rahimi, R., Ochoa, M., Pinal, R., and Ziaie, B. (2015). A Smart Capsule with GI-Tract-Location-Specific Payload Release. IEEE Trans. Biomed. Eng. *62*, 2289–2295. https://doi.org/10.1109/TBME.2015.2418340.
31. Pi, X., Lin, Y., Wei, K., Liu, H., Wang, G., Zheng, X., Wen, Z., and Li, D. (2010). A novel micro-fabricated thruster for drug release in remote controlled capsule. Sens Actuators A Phys *159*, 227–232. https://doi.org/10.1016/J.SNA.2010.03.035.
32. Song, S., Yuan, S., Zhang, F., Su, J., Ye, D., Wang, J., and Meng, M.Q.-H. (2022). Integrated Design and Decoupled Control of Anchoring and Drug Release for Wireless Capsule Robots. IEEE ASME Trans. Mechatron. *27*, 2897–2907. https://doi.org/10.1109/TMECH.2021.3125673.
33. Traverso, G., Schoellhammer, C.M., Schroeder, A., Maa, R., Lauwers, G.Y., Polat, B.E., Anderson, D.G., Blankschtein, D., and Langer, R. (2015). Microneedles for Drug Delivery via the Gastrointestinal Tract. J. Pharmaceut. Sci. *104*, 362–367. https://doi.org/10.1002/JPS.24182.
34. Abramson, A., Caffarel-Salvador, E., Soares, V., Minahan, D., Tian, R.Y., Lu, X., Dellal, D., Gao, Y., Kim, S., Wainer, J., et al. (2019). A luminal unfolding microneedle injector for oral delivery of macromolecules. Nat. Med. *25*, 1512–1518. https://doi.org/10.1038/s41591-019-0598-9.
35. Chen, W., Wainer, J., Ryoo, S.W., Qi, X., Chang, R., Li, J., Lee, S.H., Min, S., Wentworth, A., Collins, J.E., et al. (2022). Dynamic omnidirectional adhesive microneedle system for oral macromolecular drug delivery. Sci. Adv. *8*, 1792. https://doi.org/10.1126/SCIADV.ABK1792/SUPPL_FILE/SCIADV.ABK1792_MOVIES_S1_TO_S4.ZIP.
36. Huang, H., Lyu, Y., and Nan, K. (2023). Soft robot-enabled controlled release of oral drug formulations. Soft Matter *19*, 1269–1281. https://doi.org/10.1039/D2SM01624A.
37. Luo, Z., Paunović, N., and Leroux, J.C. (2021). Physical methods for enhancing drug absorption from the gastrointestinal tract. Adv. Drug Deliv. Rev. *175*, 113814. https://doi.org/10.1016/J.ADDR.2021.05.024.
38. Fox, C.B., Cao, Y., Nemeth, C.L., Chirra, H.D., Chevalier, R.W., Xu, A.M., Melosh, N.A., and Desai, T.A. (2016). Fabrication of Sealed Nanostraw Microdevices for Oral Drug Delivery. ACS Nano *10*, 5873–5881. https://doi.org/10.1021/ACSNANO.6B00809/ASSET/IMAGES/LARGE/NN-2016-00809Y_0007.JPEG.
39. Mapara, S.S., and Patravale, V.B. (2017). Medical capsule robots: A renaissance for diagnostics, drug delivery and surgical treatment. J. Contr. Release *261*, 337–351. https://doi.org/10.1016/J.JCONREL.2017.07.005.
40. Cortegoso Valdivia, P., Robertson, A.R., De Boer, N.K.H., Marlicz, W., and Koulaouzidis, A. (2021). An Overview of Robotic Capsules for Drug Delivery to the Gastrointestinal Tract. J. Clin. Med. *10*, 5791. https://doi.org/10.3390/JCM10245791.
41. Byrne, J., Huang, H.W., McRae, J.C., Babaee, S., Soltani, A., Becker, S.L., and Traverso, G. (2021). Devices for drug delivery in the gastrointestinal

tract: A review of systems physically interacting with the mucosa for enhanced delivery. Adv. Drug Deliv. Rev. *177*, 113926. https://doi.org/10.1016/J.ADDR.2021.113926.

42. Abramson, A., Caffarel-Salvador, E., Khang, M., Dellal, D., Silverstein, D., Gao, Y., Frederiksen, M.R., Vegge, A., Hubálek, F., Water, J.J., et al. (2019). An ingestible self-orienting system for oral delivery of macromolecules. Science *363*, 611–615. https://doi.org/10.1126/SCIENCE.AAU2277.

43. Lee, J., Lee, H., Kwon, S.H., and Park, S. (2020). Active delivery of multilayer drug-loaded microneedle patches using magnetically driven capsule. Med. Eng. Phys. *85*, 87–96. https://doi.org/10.1016/J.MEDENGPHY.2020.09.012.

44. Lee, J., Kim, D.i., Bang, S., and Park, S. (2022). Drug-Loaded Mucoadhesive Patch with Active Delivery and Controlled Releasing Ability. Advanced Intelligent Systems *4*, 2100203. https://doi.org/10.1002/AISY.202100203.

45. Levy, J.A., Straker, M.A., Stine, J.M., Beardslee, L.A., Borbash, V., and Ghodssi, R. (2023). Thermomechanical Soft Actuator for Targeted Delivery of Anchoring Drug Deposits to the GI Tract. Adv. Mater. Technol. *8*, 2201365. https://doi.org/10.1002/ADMT.202201365.

46. Kochhar, J.S., Quek, T.C., Soon, W.J., Choi, J., Zou, S., and Kang, L. (2013). Effect of microneedle geometry and supporting substrate on microneedle array penetration into skin. J. Pharmaceut. Sci. *102*, 4100–4108. https://doi.org/10.1002/JPS.23724.

47. Lee, J.W., Park, J.H., and Prausnitz, M.R. (2008). Dissolving Microneedles for Transdermal Drug Delivery. Biomaterials *29*, 2113–2124. https://doi.org/10.1016/J.BIOMATERIALS.2007.12.048.

48. Lowrie, W. (2023). The Earth's Magnetic Field. In The Earth's Magnetic Field (Oxford University Press).

49. Berger, A. (2002). How does it work?: Magnetic resonance imaging. BMJ Br. Med. J. (Clin. Res. Ed.) *324*, 35. https://doi.org/10.1136/BMJ.324.7328.35.

50. VI, E., IV, S., EV, P., AO, B., and RA, T. (2002). Mechanical properties of the human gastrointestinal tract. J. Biomech. *35*, 1417–1425. https://doi.org/10.1016/S0021-9290(02)00084-2.

51. Kahn, H.S., Rissanen, H., Bullard, K.M., and Knekt, P. (2014). The population distribution of the sagittal abdominal diameter (SAD) and SAD/height ratio among Finnish adults. Clin. Obes. *4*, 333–341. https://doi.org/10.1111/COB.12078.

52. Findley, W.N., and Davis, F.A. (2013). Creep and Relaxation of Nonlinear Viscoelastic Materials Revised (Courier Corporation).

53. Barducci, L., Norton, J.C., Sarker, S., Mohammed, S., Jones, R., Valdastri, P., and Terry, B.S. (2020). Fundamentals of the Gut for Capsule Engineers. Preprint at IOP Publishing Ltd, 42002. https://doi.org/10.1088/2516-1091/abab4c.

54. Straker, M.A., Levy, J.A., Stine, J.M., Borbash, V., Beardslee, L.A., and Ghodssi, R. (2023). Freestanding region-responsive bilayer for functional packaging of ingestible devices. Microsyst. Nanoeng. *9*, 61. https://doi.org/10.1038/s41378-023-00536-w.

55. Helander, H.F., and Fändriks, L. (2014). Surface area of the digestive tract - revisited. Scand. J. Gastroenterol. *49*, 681–689. https://doi.org/10.3109/00365521.2014.898326.

56. Pharmaceutical Diluents and Fillers: Overview, Types, and Uses | PharmaCentral | Materials and Knowledge Platform https://pharmacentral.com/learning-hub/technical-guides/pharmaceutical-diluents-and-fillers/.

57. Rudén, J., Frenning, G., Bramer, T., Thalberg, K., and Alderborn, G. (2021). On the relationship between blend state and dispersibility of adhesive mixtures containing active pharmaceutical ingredients. Int. J. Pharm. X *3*, 100069. https://doi.org/10.1016/J.IJPX.2020.100069.

58. Katona, M.T., Kakuk, M., Szabó, R., Tonka-Nagy, P., Takács-Novák, K., and Borbás, E. (2022). Towards a Better Understanding of the Post-Gastric Behavior of Enteric-Coated Formulations. Pharm. Res. (N. Y.) *39*, 201–211. https://doi.org/10.1007/S11095-021-03163-0/TABLES/6.

59. Cutnell, J., and Johnson, K. (1998). Physics, 4th Edition (John Wiley & Sons, Inc.).